Imaging and Sounding of Ice Fields With Airborne Coherent Radars

CHARLES ELACHI AND WALTER E. BROWN, JR.

Jet Propulsion Laboratory Space Sciences Division, California Institute of Technology, Pasadena, California 91103

Airborne coherent radar observations of ice fields conducted in the last 4 years are presented and discussed These observations contain radar imagery of glaciers in southeast Alaska imagery of coastal and ea ce n northern Alaska and the Beaufort Sea. and sounding f layered ntinenta e in Green and

INTRODUCTION

The recent development of the synthetic aperture imaging radar [*Brown and Porcello* 1969 *Harger* 1970 *Rihaczek* 1969] which generates high-resolution surface imagery from an airborne or spaceborne platform, has generated interest in the scientific community for its use as an all-time all-weather remote sensor to study the earth s solid surface, oceans. and polar regions [*Bradic* 1967· *Waite and MacDonald*. 1970· *Brown et al* 1973] The radar echo is a signature of the characteristics of the reflecting surface and immediate subsurface layer roughness slope distribution dielectric constant and layering The penetration property of the radio waves allows a radar system to detect subsurface layers

A unique capability of the imaging radar is that it is an all-weather all-time sensor because it provides its own illumination and usually operates in the microwave region of the electromagnetic spectrum to which clouds are transparent

In this paper we present a number of observations collected with the Jet Propulsion Laboratory (JPL) *L* band (i.e., 25-cm wavelength) imaging radar and VHF (2-m wavelength) sounder Specific data presented are sounding data taken over Greenland showing layering down to a depth of about 100 m and radar imagery of glaciers in southeast Alaska, near-coast ice in northern Alaska, and sea ice cover in the Beaufort Sea.

The radar imagery shows a strong similarity to photographic imagery in many cases and differences in some cases. The conclusion of our observations is that the imaging radar sensor and photographic cameras are complementary and that the radar is a valuable sensor in its own right. especially because of its unique capabilities. all-weather all-time capability and high resolution independent of the height of the platform (aircraft or spacecraft).

COHERENT RADAR IMAGING AND SOUNDING PRINCIPLE

The resolution u of a UV, optical, or IR sensor is proportional to the operating wavelength λ, the platform height H, and the inverse of the aperture size d, i.e.,

$$u \sim \lambda H/d \qquad (1)$$

The resolution achievable in these regions of the spectrum can be very small (in the range of a few meters) even from spacecraft altitudes. In the microwave region the resolution is drastically degraded because of the longer wavelength. The aperture size could be increased within reasonable limits, however, a high imaging resolution with microwaves can be achieved only from relatively low flying aircrafts. The coherent radar synthetic aperture technique circumvents this limitation by using the platform (aircraft or spacecraft) motion to generate an effective aperture far larger than the real aperture As a matter of fact, the theoretical resolution achievable is independent of the height For more details see *Harger* [1970] and *Rihaczek* [1969].

Most imaging radars operate in the centimeter region and at grazing incidence angles. However, the imagery presented in this paper was collected with a 25 cm radar operating at near vertical incidence The brightness in the radar image is proportional to the local radar backscatter cross section which in turn is related to the surface roughness, slope distribution and dielectric constant [*Barrick*, 1968, *Barrick and Peake* 1968.

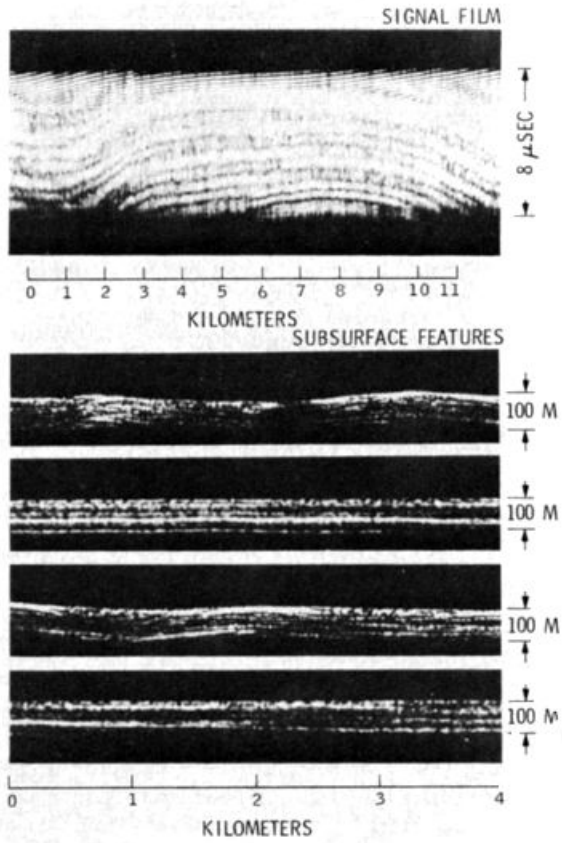

Fig. 1 Subsurface layers in the Greenland continental ce The upper image corresponds to the radar data collected during the flight before processing. The lower images are four successive sections of the processed data of a continuous strip covering a 16-km line. Up to 12 layers were detected in the upper 100 m. In the upper section finger rafting' between the layers can be seen

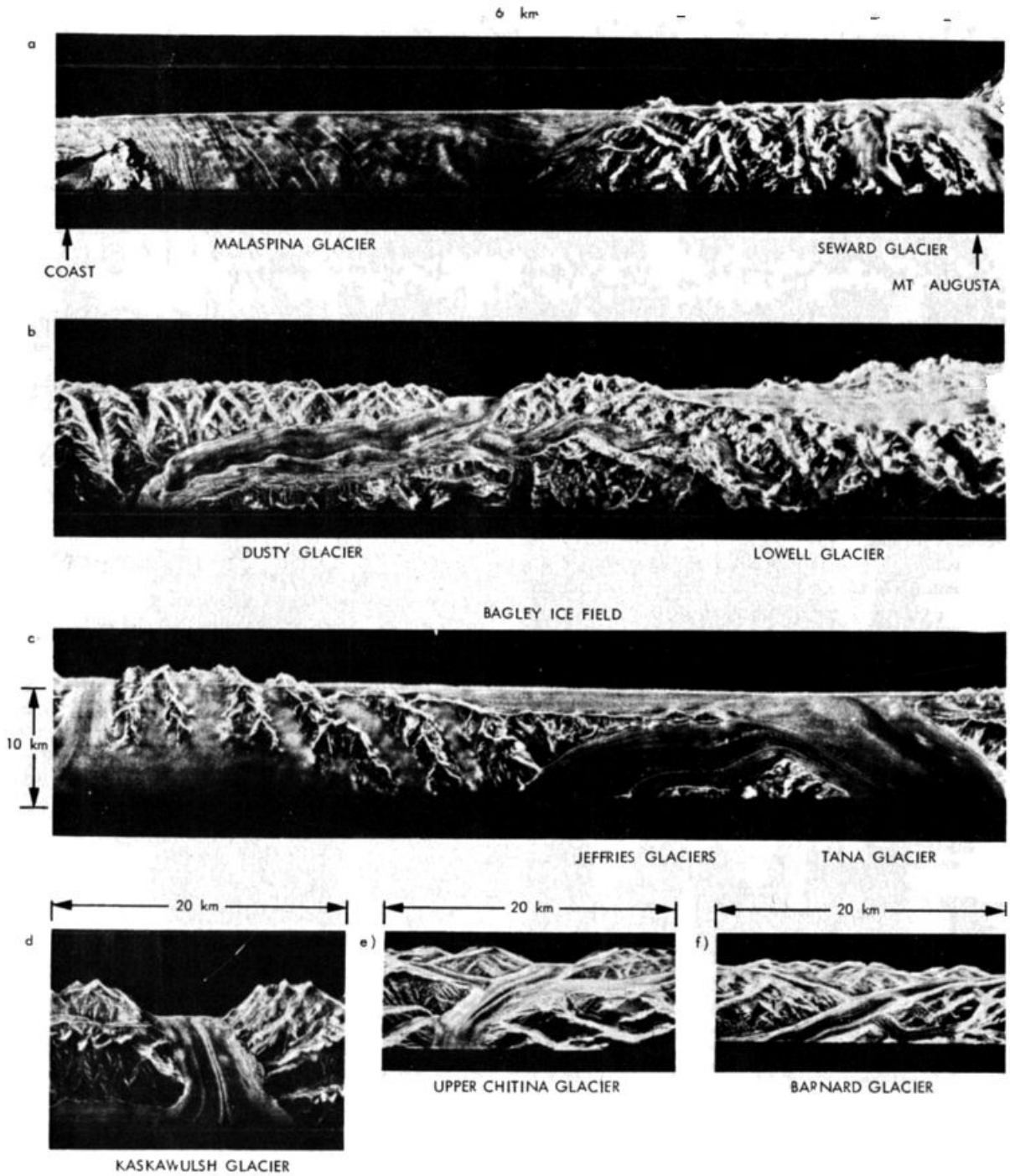

Fig. Radar imagery of a number of glaciers in southern Alaska. Each trace is corrected for aircraft altitude variations with respect to a 10 km altitude. The bright line corresponds to the specular echo from the nadir thus corresponding to the ground track of the aircraft. The image to one side of the line of flight (see Figure 4 for geometry).

Kirshen 1971]. For instance, a ridge of a flow in an ice field will be imaged as a bright linear zone because the chaotic rough ice will backscatter strongly the electromagnetic wave. New ice will be imaged with a tone different from that of old ice because of the change in surface roughness. Similarly, in glacier imagery linear moraines and surface ripplings are clearly seen with sharply different tones.

To achieve subsurface sounding longer wavelengths have to be used. We conducted our observation with a 7 m coherent radar (prototype of the Apollo 17 lunar sounder [*Porcello et al.* 1974]) over Greenland to sound the continental ice sheet. Any dielectric discontinuity would reflect an echo. Deep sounding can be achieved in low loss continental ice fields but not in sea ice.

Observations

Continental ice sounding. During airborne flight tests over Greenland in August 1972 the Apollo 17 lunar sounder radar detected many dielectric discontinuities in the top layer of the ice cover (Figure 1). These discontinuities appeared layerlike

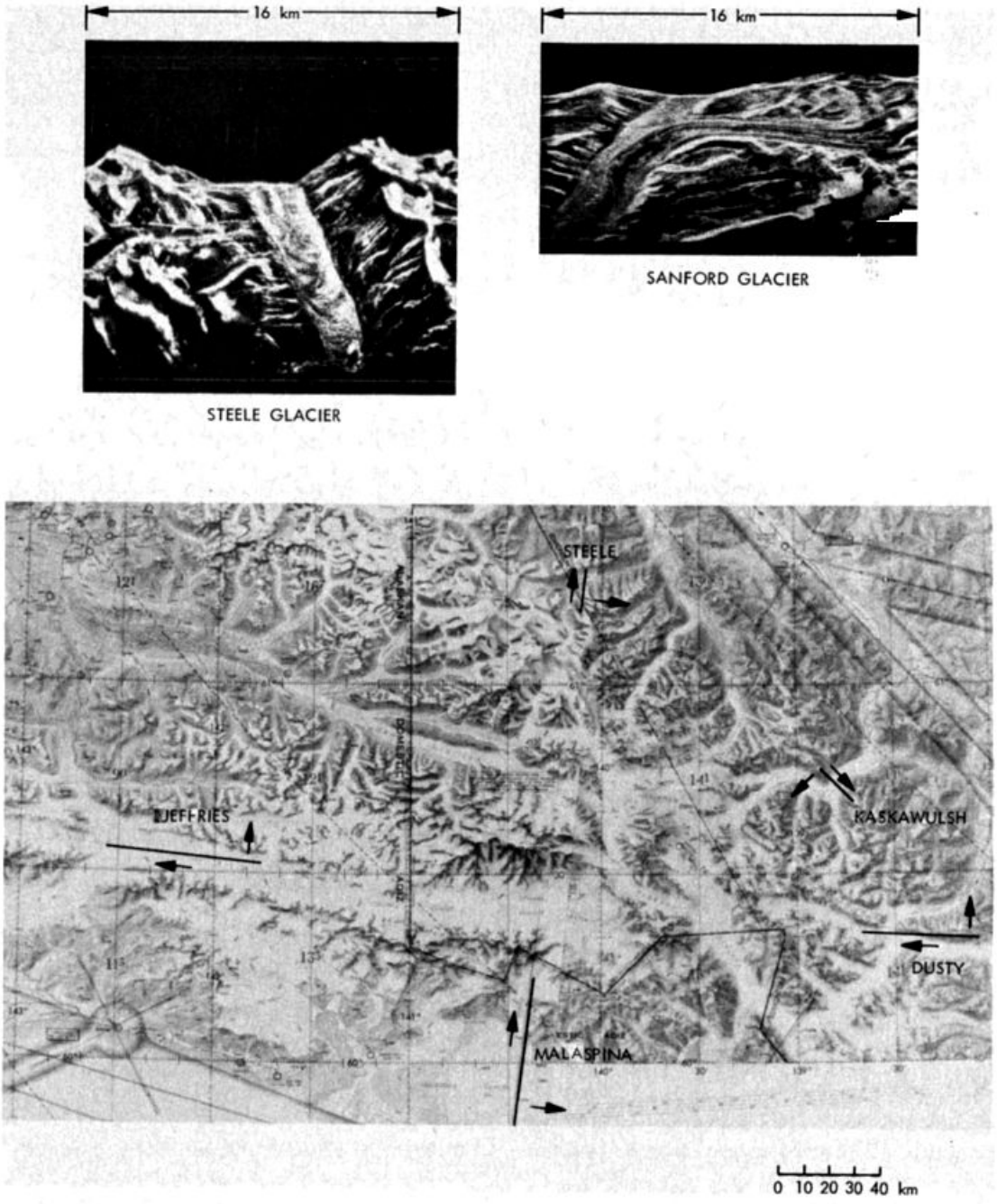

Fig. 3. Radar imagery of two glaciers and a topographic map showing the location of some of the glaciers that were imaged. The lines correspond to the line of flight, and the two arrows show the flight direction and the imaged side (always to the right of the aircraft).

and were detected over most of Greenland. The flight path extended from the northwest coast (60° longitude, 70° latitude) to the southern coast (40°12′ longitude, 60°30′ latitude) in a zigzag pattern down the central region of Greenland.

The in-depth sounding range was about 100 m below the surface (an estimated 200 years of accumulation), and a dozen layers can be seen on the processed data (Figure 1). Some of these layers reflected the electromagnetic wave even more than the surface. The operating wavelength was 2 m (150 MHz) and the large penetration is due to the low loss in the continental ice.

Because of the radar reflection is a discontinuity in the dielectric constant, however, the reason for this discontinuity [illegible] known at this time. An interesting observation is that some areas finger rafting seems to exist leading to the speculative suggestion of relative transverse motion of different layers.

It should be emphasized that the VHF sounder used in our experiment is a synthetic aperture radar that provides very high resolution both in depth (a few meters) and along the line of flight (about 15 m). Thus it is complementary to other radar sounders that use a brute force technique (Gudmansen [illegible] and have lower resolution near the surface (for 100 m, and deeper penetration capability of 1 km or more) (*Evans and Robin*, 1966; *White*, 1970; *Robin et al.*, 1970).

Glacier imaging [illegible] the 2-cm radar [illegible]

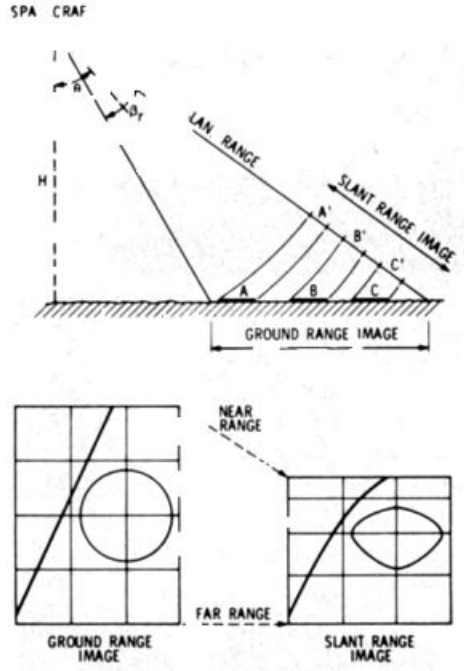

Fig. 4. Geometry of radar imagery. The radar measures the time delay (i.e. range) to a specific feature. Thus the ground image is projected on a time line called the slant range. Near-range features are compressed relative to far-range features. This distortion can be removed easily by digital processing. The platform could be an aircraft or a spacecraft.

the objective of imaging glaciers. The approximate area covered extended from 59°30′ to 62° latitude, and 138°45′ longitude. A sample of this imagery showing a variety of glaciers and the corresponding topographic map are shown in Figures 2 and 3.

The geometry of radar imaging is different from that of photographic imagery. The radar imagery corresponds to an angle-time delay instead of the angle-angle geometry of standard photography (Figure 4). The bright line in the upper part of the radar image is the echo from the nadir. Thus it corresponds to a profile of the surface along the flight track. The rest of the image corresponds to a swath of 10 km to the right of the flight track. However it is projected on the radar line (Figure 4) and thus leads to some image geometric distortion particularly at near-vertical look angles.

Figure 2*a* is a radar image of the eastern part of the Malaspina piedmont glacier. The line of flight was on the eastern edge of the Seward glacier. It is well known that the entering ice from the Seward glacier is forced into impressive horizontal fold patterns of fantastic scale and complexity by the stagnant frontal area along the coast. These folds are clearly seen on the radar imagery, and they are comparable to what is seen photographically [*Gilluly et al.*, 1968]. These folds start at the Seward glacier entrance and form large curvilinear lines that become parallel to the coast (at the left of Figure 2*a*). The width of the radar image swath in Figure 2*a* is about 10 km.

Figure 2*b* is a radar image of the Dusty glacier that clearly shows its boundaries and the medial moraine from the tributary at the left. The ridge of medial (below the junction) and lateral moraine is also clearly seen in the image of the Tana-Jeffries glaciers (Figure 2*c*). The Kaskawulsh, upper Chitina, and Anderson glaciers imagery (Figures 2*d*, *e* and *f*) shows most dramatically the moraine patterns in branching valley glacier systems.

The moraine ridges are clearly seen on radar imagery because of the change in roughness and the chaotic state of the ice at the boundary between the two flowing ice masses and because of the change of the dielectric constant due to the dirty ice and loose rocks. In the above imagery we can also see large patches of different tones (Figures 2*a*, *b*, and *c*) indicating variation in the surface roughness.

Figure 3 shows a topographic map of the area imaged during the flights and the radar image (blown up) of the Steele and Sanford glaciers. The Steele glacier shows clearly the concave profiles of the ice flow that result from the differential motion of the ice across the glacier. The Sanford glacier shows clearly the moraine system and the transverse ripples all the way down the glacier flow line.

Coastal sea ice. A number of flights were conducted over the north Alaskan coast and the Beaufort Sea in conjunction with the Aidjex mission. Figure 5 shows radar imagery of coastal sea ice. The location of the coast is 69°36′ latitude and 140°15′ longitude, and the flight line was to the north northwest. The coastline can be seen clearly, and three successive boundary parallels to the coast were detected. These boundaries were detected during many flights over a large section of the coastline, and they most probably correspond to flaw zones separating different regions of fast ice and pack ice. The chaotic state of the ice in these narrow zones leads to increased surface roughness, resulting in a stronger radar return.

Next to the shore a large number of medium and small sized flows can be seen. No sizable fracturing or ridging is present in the fast ice region. Farther away from the coast many young ice flows (dark to black tones) are present in large areas of ridged old ice (light tones). Some new ice flows have ridges

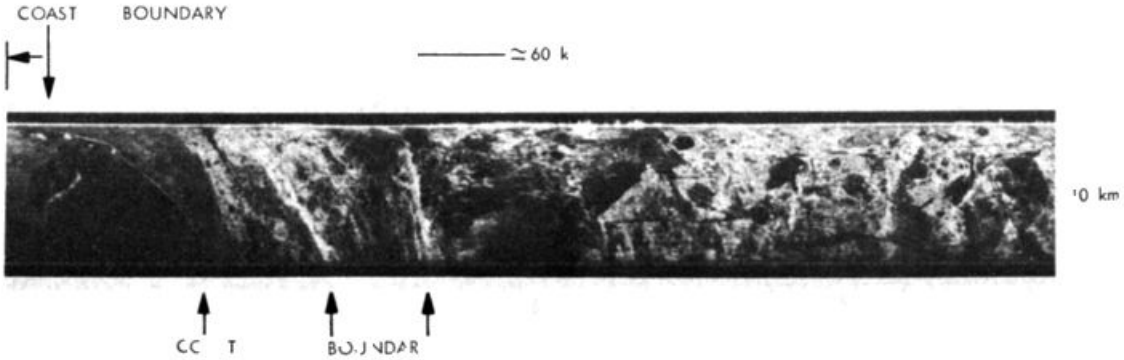

Fig. 5. Radar image of coastal ice in northern Alaska. The coast is at the left. Three ice boundaries (flaws) can be seen to its right. A large number of flows and ridges can be seen in the fast ice and pack ice areas.

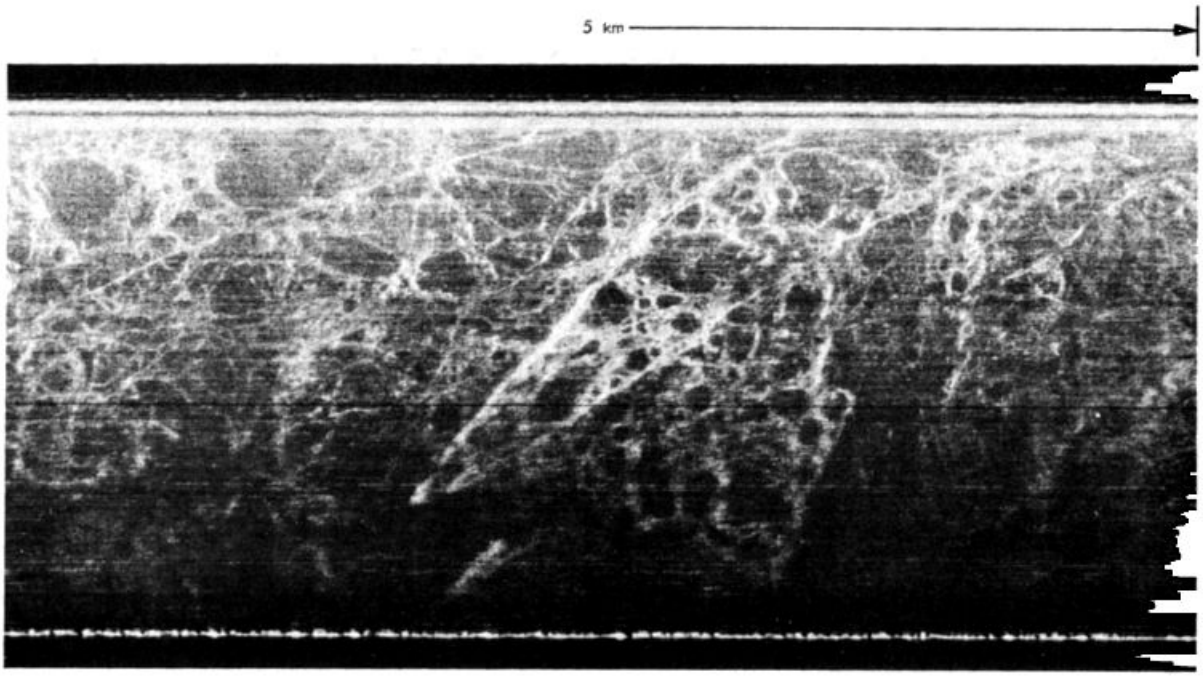

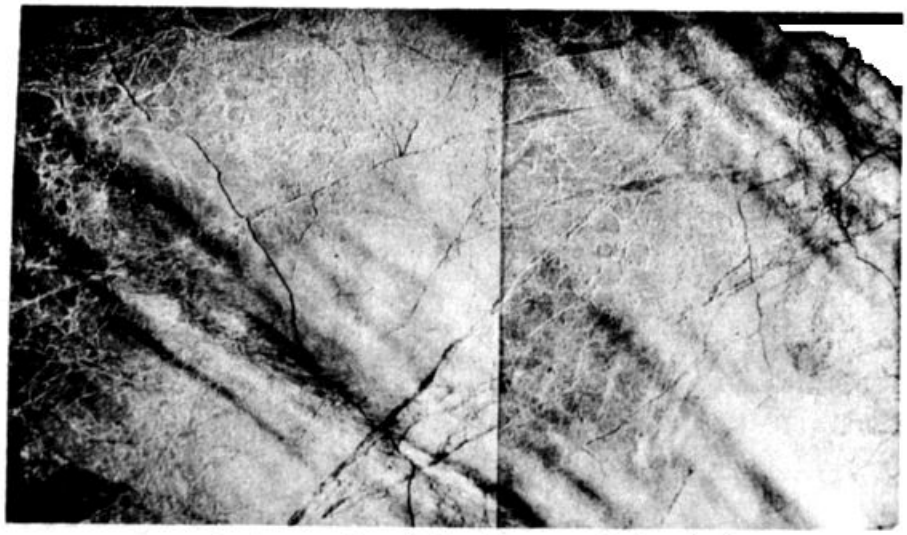

Fig. 6 Sea ice radar and photo imagery in the Beaufort Sea

across them The large dark areas are most probably open water

The interpretation of radar ice imagery is still in its infancy. Some work has been conducted recently toward this objective (Raytheon Company) [*Bradic* 1967] and it seems that general criteria for the identification of ice types can be generated However, more comparative work is still needed

Sea ice. In Figures 6 and 7 we show radar and photo imagery of two areas in the Beaufort Sea A large number of features can be seen on both images however the radar imagery seems to be better in detecting and mapping pressure ridges and delineating ice flows. It appears that the radar visibility of a ridge is enhanced because the radio wave penetrates the drifting snow that tends to hide the ridge in the photographs may also be possible that the radar waves are reflected from broken ice (scatterers) buried in the ridge system. In fact, the ridge width appears to be of the order of 100–200 m on radar imagery. This is an order of magnitude larger than surface ridges seen on the photograph

On the other hand, photo imagery seems to be better in the detection of leads However, other experimenters have mapped leads by using near-grazing [*Johnson and Farmer* 1971] Ku band imaging radars.

CONCLUSION

In this paper we presented a small sample of radar imagery of glaciers, sea ice, and coastal ice fields and sounding data of continental ice collected with airborne synthetic aperture radars. Our understanding of the radar image of ice and its comparative interpretation is

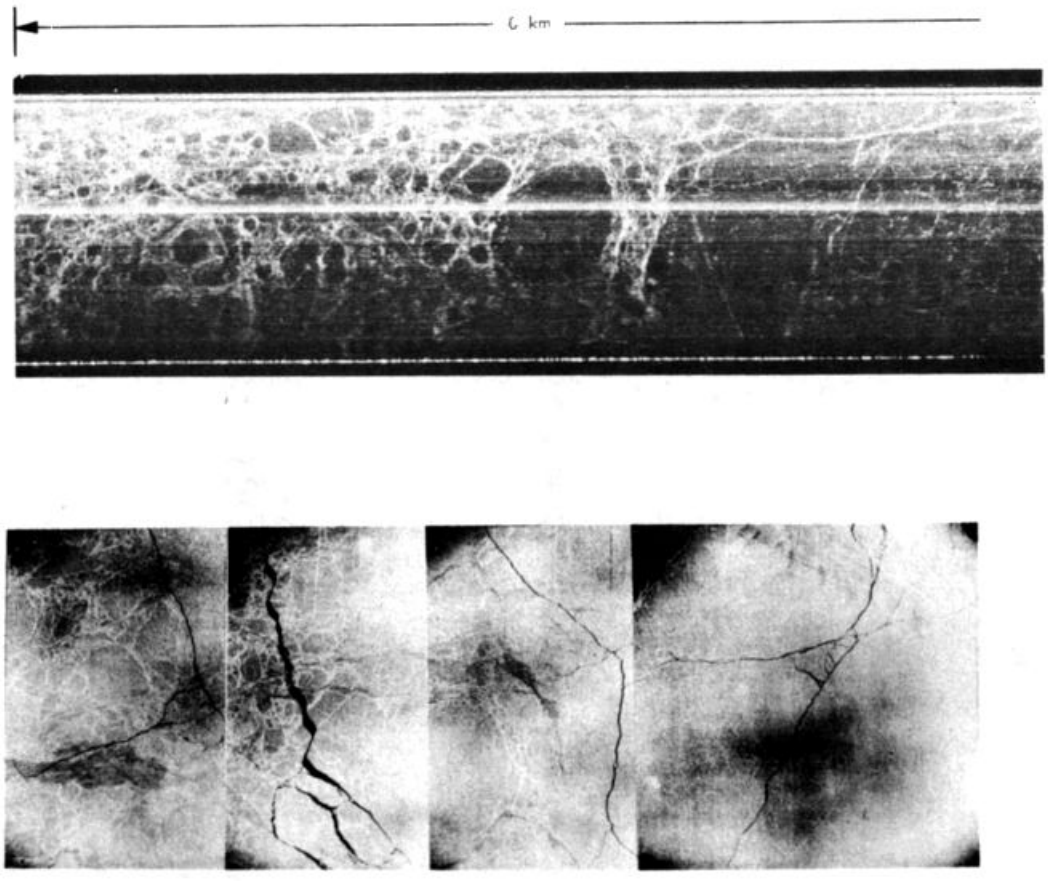

Fig. 7 Sea ice radar and photo imagery in the Beaufort Sea.

work is definitely needed. However, the imaging sounding radar seems to have significant potential as a remote sensor in the field of glaciology and polar ice study. It is an all-weather all time system, and the presence of cloud cover, which is common in the polar areas, has no effect at all on the radar performance (some of the imagery presented in this paper was taken during complete cloud coverage). Another factor is that the altitude of the platform has little effect on the image resolution. Thus similar imagery but with a much wider swath width can be obtained from orbiting spacecraft and will provide a far greater polar region coverage.

In many cases the radar shows most of the features seen in a photograph. Thus both systems can be considered as complementary because the radar would extend the imaging capability to the whole year regardless of cloud cover. This is important in the study of the dynamics of glaciers and ice covers. On the other hand, the radar sounder is basically the only system that can probe large areas in a reasonable amount of time and thus it can be used simultaneously with local direct sounding.

Finally it should be mentioned that the imaging and/or sounding radar system has unique remote sensing capabilities for planetary exploration as well as for earth studies. Great interest has recently been generated in the polar cap of Mars as a result of the Mariner Mars 1971 mission. The Martian polar caps are believed to consist of layers of water ice, dry ice, and dust. An orbiting radar sounder would be a powerful technique for mapping this layering.

Acknowledgments. We wish to thank T. W. Thompson [illegible] helpful discussions and would also like to thank the members of the Science Radar Group, A. Laderman, E. Caro, and W. Skotnick, all from JPL, who contributed to collecting the data in this paper. This paper presents the results of one phase of research carried out at JPL, California Institute of Technology, under contract NAS7-100, sponsored by the National Aeronautics and Space Administration.

REFERENCES

Barrick, D. E., Rough surface scattering based on specular point theory, *IEEE Trans. Antennas Propagat.*, *AP16*, 449–454, 1968.

Barrick, D. E., and W. H. Peake, Review of scattering from surfaces with different roughness scales, *Radio Sci.*, *3*, 865–868, 1968.

Bradie, R. A., SLAR imagery for sea ice studies, *Photogramm. Eng.*, *33*, 63–66, 1967.

Brown, W. E., C. Flachi[illegible] and T. W. Thompson, Ocean glaciographic observations with imaging radar, paper presented at Fall Meeting, Un[illegible] Radio Sci. Int., Boulder, Colo., August 19[illegible]3.

Evans, S., and G. de Q. Robin, Glacier depth sounding from the air, *Nature*, *210*, 883–885, 1966.

Gilluly, J., A. C. Waters, and A. O. Woodford, *Principles of Geology*, W. H. Freeman, San Francisco, Calif., 1968.

Harger, R. O., *Synthetic Aperture Radar Systems*, Academic, New York, 1970.

Johnson, J. D., and I. D. Farmer, Use of side looking airborne radar for sea ice detification, *J. Geophys. Res.*, *76*, 1821–1825, 1971.

Krishen, K., Correlation of radar backscattering cross sections with ocean wave height and wind velocity, *J. Geophys. Res.*, *76*, 6528–6539, 1971.

Porcello, L. R., Jordan, J. S. Zelenka, G. F. Adams, R. J. Phillips, W. E. Brown, Jr., S. H. Ward, and P. L. Jackson, The Apollo lunar sounder system, *Proc. IEEE*, *62*, 769–783, 1974.

Rihaczek, A. W., *Principles of High Resolution Radar,* McGraw-Hill, New York, 1969.
Robin, G. de Q., S. Evans, D. J. Drewry, C. H. Harrison, and D. L. Petric, Radio-echo sounding of the Antarctic ice sheet, *Antarctic J. U.S., 5,* 229–232, 1970.
Waite, A. H., Jr., International experiment in glacier sounding, 1963 and 1964, *Can. J. Earth Sci., 3,* 887–892, 1966.
Waite, W. P., and H. P. MacDonald, Snowfield mapping with K-band radar, *Remote Sensing, 1,* 143–150, 1970.

(Received July 29, 1974;
revised November 20, 1974;
accepted December 10, 1974.)